

Functional Organization of Squirrel Monkey Primary Auditory Cortex: Responses to Pure Tones

STEVEN W. CHEUNG,¹ PURVIS H. BEDENBAUGH,² SRIKANTAN S. NAGARAJAN,³ AND CHRISTOPH E. SCHREINER¹

¹*Coleman Memorial Laboratory and W. M. Keck Center for Integrative Neuroscience, Department of Otolaryngology, University of California, San Francisco, California 94143-0342;* ²*Departments of Neuroscience and Otolaryngology, University of Florida Brain Institute, Gainesville, Florida 32610-0244;* and ³*Department of Bioengineering, University of Utah, Salt Lake City, Utah 84112-9458*

Received 25 August 2000; accepted in final form 6 December 2000

Cheung, Steven W., Purvis H. Bedenbaugh, Srikantan S. Nagarajan, and Christoph E. Schreiner. Functional organization of squirrel monkey primary auditory cortex: responses to pure tones. *J Neurophysiol* 85: 1732–1749, 2001. The spatial organization of response parameters in squirrel monkey primary auditory cortex (AI) accessible on the temporal gyrus was determined with the excitatory receptive field to pure tone stimuli. Dense, microelectrode mapping of the temporal gyrus in four animals revealed that characteristic frequency (CF) had a smooth, monotonic gradient that systematically changed from lower values (0.5 kHz) in the caudoventral quadrant to higher values (5–6 kHz) in the rostrorodorsal quadrant. The extent of AI on the temporal gyrus was ~4 mm in the rostrocaudal axis and 2–3 mm in the dorsoventral axis. The entire length of isofrequency contours below 6 kHz was accessible for study. Several independent, spatially organized functional response parameters were demonstrated for the squirrel monkey AI. Latency, the asymptotic minimum arrival time for spikes with increasing sound pressure levels at CF, was topographically organized as a monotonic gradient across AI nearly orthogonal to the CF gradient. Rostral AI had longer latencies (range = 4 ms). Threshold and bandwidth co-varied with the CF. Factoring out the contribution of the CF on threshold variance, residual threshold showed a monotonic gradient across AI that had higher values (range = 10 dB) caudally. The orientation of the threshold gradient was significantly different from the CF gradient. CF-corrected bandwidth, residual Q10, was spatially organized in local patches of coherent values whose loci were specific for each monkey. These data support the existence of multiple, overlying receptive field gradients within AI and form the basis to develop a conceptual framework to understand simple and complex sound coding in mammals.

INTRODUCTION

Many microelectrode studies have examined the response properties of primate auditory forebrain neurons to simple sound stimuli, most notably characteristic frequency (CF) topography in Old and New World monkeys (Aitkin et al. 1986; Imig et al. 1977; Kosaki et al. 1997; Luethke et al. 1989; Merzenich and Brugge 1973; Morel and Kaas 1992; Morel et al. 1993; Rauschecker et al. 1997; Recanzone et al. 1999). While CF is an important organizational principle, it is only

one of many stimulus dimensions that are potentially encoded in cortex. Knowledge of spectral and temporal response properties of cortical neurons beyond CF will enhance understanding of how simple and complex sounds are represented in the forebrain, and such a description is a goal of this study. This information is essential to constructing an ensemble of basic response descriptors that can reveal principles for encoding complex, behaviorally significant communication sounds, such as species specific vocalizations and speech.

This study and its companion (P. H. Bedenbaugh, S. W. Cheung, C. E. Schreiner, S. S. Nagarajan, and A. Wong, unpublished data) focus on the functional organization of squirrel monkey (*Saimiri sciureus*) primary auditory cortex (AI) by documenting the spatial and temporal organization of responses to tone burst and rate-varying click train stimuli. Tone bursts are specific in frequencies and extended in time, while clicks are extended in frequencies and specific in time. Together, they provide a more complete picture of how spectral and temporal aspects of simple sounds are represented in AI. The rationale for an in-depth study of primate AI is threefold. First, AI serves as one principal tract of the lemniscal auditory system. Second, a large body of literature on encoding dimensions is already available for feline AI, which provides a basis for interspecies comparisons. Finally, AI is a source for corticocortical connections to ipsilateral fields (Luethke et al. 1989; Morel and Kaas 1992; Morel et al. 1993; Rouiller et al. 1991). Understanding how it represents, processes, and transforms auditory information is a critical step in understanding the hierarchical and parallel nature (Rauschecker et al. 1995, 1997) of auditory forebrain function.

Single- and multiunit studies of mammalian auditory forebrain neuronal responses to tonal stimuli found an orderly representation of CF in cat and primate (Aitkin et al. 1986; Imig et al. 1977; Luethke et al. 1989; Merzenich and Brugge 1973; Merzenich et al. 1975; Morel and Kaas 1992; Phillips and Irvine 1982; Phillips and Orman 1984; Reale and Imig 1980; for review, Clarey et al. 1992; Morel et al. 1993; Recanzone et al. 1999). Other dimensions, such as intensity-dependent coding and extent of excitatory receptive fields,

Address for reprint requests: S. W. Cheung, Div. of Otolaryngology, Neurotology, and Skull Base Surgery, Box 0342 A730 400 Parnassus Ave., San Francisco, CA 94143-0342 (E-mail: cheung@phy.ucsf.edu).

The costs of publication of this article were defrayed in part by the payment of page charges. The article must therefore be hereby marked "advertisement" in accordance with 18 U.S.C. Section 1734 solely to indicate this fact.

have complex spatial patterns (Heil et al. 1992, 1994; Recanzone et al. 1999; Schreiner 1995; Schreiner and Sutter 1992) along isofrequency contours. Many auditory fields are present (Imig et al. 1977; Knight 1977; Merzenich and Brugge 1973; Phillips and Irvine 1982; Phillips and Orman 1984; Rauschecker et al. 1995, 1997); these appear physiologically as gradient reversals in tonotopic organization or by the virtual absence of tonotopic organization (Merzenich and Schreiner 1992; Rauschecker et al. 1995, 1997; Schreiner and Cynader 1984). In many species, the isofrequency contour is traversed by binaural interaction bands (Imig and Adrián 1977; Kelly and Judge 1994; Middlebrooks et al. 1980; Recanzone et al. 1999) or interleaved with neurons sensitive to azimuthal location (Clarey et al. 1994). In the visual cortex and in the bat auditory forebrain, the role of multiple field representation of sensory stimuli supports the notion of hierarchical refinement and increasing functional specialization. There is only sparse information on the specific role and contribution of multiple auditory fields in cats and monkeys.

Several studies of squirrel monkey auditory cortex (Bieser 1998; Bieser and Mueller-Preuss 1996; Funkenstein and Winter 1973; Hind 1972; Newman and Symmes 1974, 1979; Pelleg-Toiba and Wollberg 1989; Shamma and Symmes 1985) have revealed some response properties of neurons to simple and complex sounds. However, these studies provide limited information on the number or physiologic boundaries of auditory fields and the representation of simple sounds. While cortical representations of species-specific vocalizations were examined (Bieser 1998; Newman and Symmes 1974; Winter and Funkenstein 1973), no detailed microelectrode mapping study has characterized auditory field boundaries under precise topographical control. Studies indicate that squirrel monkey AI location (Bieser and Mueller-Preuss 1996; Burton and Jones 1976; Funkenstein and Winter 1973; Jones and Burton 1976; Massopust et al. 1968; Winter and Funkenstein 1973) is similar to that in other New World monkeys (Aitkin et al. 1986; Imig et al. 1977; Luethke et al. 1989; Morel and Kaas 1992; Recanzone et al. 1999); namely, a portion of AI is found on the lateral surface of the temporal gyrus. By densely mapping the temporal gyrus, which is the most accessible portion of primary auditory cortex, we can learn more about the details of functional topography and gain insight into computational map constructs in the primate forebrain (Knudsen et al. 1987).

The current study relies on comprehensive, high-density sampling of entire isofrequency bands within primary auditory cortex of single animals, without pooling data across subjects. Mapping the temporal gyrus samples a limited range of CF values but captures the full variability of responses over a large area (~10 mm²). Individual differences are considered in the context of common patterns of variations in neuronal response parameters. This approach reveals population profiles while preserving individual patterns.

The results show variable scatter of receptive field parameters locally but nonhomogeneous and nonrandom spatial distributions of several response properties beyond CF globally. This suggests that squirrel monkey AI is organized along systematic, multiple independent gradients and subregions with specialized spectral and temporal receptive field characteristics.

METHODS

Surgical preparation

Four young adult, male squirrel monkeys were used in accordance with an approved institutional protocol and congruent with applicable international, national, state, and institutional welfare guidelines. Inhalation of a halothane:nitrous oxide:oxygen (2:48:50%) mixture was used to reach a surgical plane of anesthesia. Skin overlying the trachea, stereotaxic pin sites and scalp were injected with Lidocaine 2%. Tracheotomy was performed to secure the airway and intravenous (iv) access was established in the saphenous vein. Subsequently, inhalational agents were discontinued, and iv pentobarbital sodium (15–30 mg/kg) was administered and titrated to effect for the duration of the experiment. Normal saline with 1.5% dextrose and 20 mEq KCl delivered at 6–8 ml/kg/h supported cardiovascular function. Ceftizoxime (10–20 mg/kg iv every 12 h), a third-generation cephalosporin antibiotic that crosses the blood-brain barrier was given for prophylaxis against infection. Core temperature was monitored with a thermistor probe and maintained at ~38°C with a feedback-controlled heated water blanket. Electrocardiogram and respiratory rate were monitored continuously throughout the experiment.

The head was stabilized with a customized fixation device that permitted access to the external auditory meati. A scalp incision was followed by soft tissue mobilization to expose the temporoparietal cranium. Burr holes over the auditory forebrain were positioned extradurally, and a bone plate was removed. The dura was reflected to expose temporal lobe ventral to the lateral sulcus. The brain was kept moist with silicone oil. A magnified video image of the recording zone was captured with a camera and stored in a microcomputer for identifying penetrations during the experiment. At the conclusion of each study, the animal was euthanized with pentobarbital sodium (150 mg/kg iv), followed by transcardial perfusion with a formaldehyde/glutaraldehyde mixture for brain fixation.

Stimulus generation

Experiments were performed in a double-walled sound-attenuating chamber (IAC). Auditory stimuli were delivered through a headphone (STAX-54) enclosed in a small chamber that was connected via a sealed tube into the external acoustic meatus of the contralateral ear (Sokolich, U.S. Patent 4251686; 1981). The sound-delivery system was calibrated with a sound meter (Brüel and Kjær 2209) and waveform analyzer (General Radio 1521-B). The frequency response of the system was flat within 6 dB up to 14 kHz, which encompassed the majority of neurons studied. The output rolled off at 10 dB/octave above 14 kHz.

Tone bursts (3-ms linear rise/fall; total duration, 50 ms; and interstimulus interval, 400–1,000 ms) were generated by a microprocessor (TMS32010, 16-bit D-A converter at 120 kHz). The CF was estimated for each penetration by using the quietest search tone burst frequency that evoked spike activity above the spontaneous level. Frequency-level response areas were recorded by presenting 675 pseudo-randomized tone bursts at different frequency and sound pressure level (SPL) combinations. The frequency-level pairs spanned 2.5–77.5 dB SPL in 5-dB steps, and 45 frequencies in logarithmic steps across a 2- to 4-octave range, centered on the neuron's estimated CF. One tone burst was presented at each frequency-level step (Schreiner and Mendelson 1990).

Recording procedure

All mapping experiments were performed on the left hemisphere. Parylene-coated tungsten microelectrodes (Microprobe and FHC) with 1–2 M Ω impedance at 1 kHz were used for single- and multiunit recordings at depths 650–950 μ m, corresponding to cortical layers III and IV. Microelectrodes aligned perpendicular to the cortical surface were lowered with a hydraulic microdrive (Kopf) guided by a depth

counter. Action potentials were isolated from background noise with an on-line window discriminator (BAK DIS-1). The number of discriminated spikes and times of arrival that occurred within a 200-ms epoch after tone burst onsets were recorded digitally. In responsive electrode tracks, only one site was studied in detail at the targeted depth range. The underlying assumption is that the response parameters in this study are rather similar for all neurons in the same vertical column of the middle cortical layers. However, when no apparent acoustically driven responses were elicited at the targeted depth range, several recording sites within a single track were probed to confirm the unresponsiveness of the column. Such penetrations were marked nonresponsive (NR).

Data analysis

At each penetration site, responses from 675 frequency-level stimulus conditions determine the frequency response area (Sutter and Schreiner 1991, 1995), including the excitatory tuning curve. Tone burst frequencies are spaced logarithmically with the range of test frequencies chosen according to the estimated CF and excitatory bandwidth. There is equal sizing and spacing of elements within this frequency-level grid. The number of recorded spikes and their arrival times evoked by the corresponding tone burst at a specific sound level are stored in a microcomputer for off-line analysis. Typically, a brief phasic discharge is recorded 8–40 ms after tone burst onset for a frequency range within the excitatory tuning curve boundary. On occasion, more dispersed discharges occurring beyond this time interval are encountered. In this account, only responses from 8 to 40 ms integrated over this time period are included. Episodes with longer latencies are associated either with locations outside AI or with oscillatory responses.

Four measures are derived from each excitatory tuning curve (Schreiner and Mendelson 1990). These are CF, minimum latency, minimum threshold, and Q10, a measure of excitatory bandwidth. CF is the frequency of the tone that evokes a response at minimum threshold. Latency is the asymptotic minimum of first spike time arrivals across the full range of stimulus levels at CF. At progressively higher intensities, the timing for first spike arrival reaches or approaches a minimum plateau (Heil 1997; Mendelson et al. 1997). Minimum threshold (hereafter, “threshold”) is the SPL of the quietest tone burst that evokes a response. The bandwidth of the excitatory receptive field is calculated from measurements of the upper and lower frequencies bounded by the tuning curve at 10 dB above minimum threshold. Q10 is calculated by dividing CF by the linear bandwidth at 10 dB above minimum threshold.

The goal of this study is to determine what other response parameters complement frequency decomposition in cortical representation of simple tones. The conceptual framework for this perspective is that auditory computations are organized as receptive field maps that overlap in cortical space, and neighboring points in these maps play, on average, incrementally different roles.

The tonotopic gradient established at the basilar membrane is reflected strongly in AI (Woolsey and Walzl 1942) and is taken into account for the evaluation of other receptive field parameters by using a decorrelation procedure. Co-variation of response parameters with CF thus is accounted for and removed using a statistical procedure prior to final reconstruction of spatial maps. The CF dependence of each parameter is fitted with a nonparametric, local regression model. This approach is chosen because while the relationship between CF and other response parameters is globally smooth, there is no basis for assuming that the fit has a particular parametric form. The local regression model adapts itself to the observed distribution of data values. Predicted values from the regression model are subtracted from experimentally observed values to yield residual, CF-independent values. Finally, the data structure of these residuals is analyzed to derive response maps. The null hypothesis predicts a uniform/random spatial distribution for each receptive field parameter in AI. A non-

parametric ANOVA is used to test the null hypothesis. Further, the fraction of total variability captured by the model is computed.

Spatial maps for the tuning parameters CF, latency, threshold, and Q10 parameters are reconstructed by Voronoi-Dirichlet Tessellation (package DELDIR, Statlib, Carnegie Mellon University). In such a tessellation reconstruction, the cortical surface is divided into a number of polygons, one for each recording site. The shape and bounded area of each polygon is determined by minimizing the cumulative perimeter of all polygons using an optimization algorithm. Each polygon reflects, with its size, the cortical area represented by the recording site and, with its color, the value of the response parameter. Small polygons indicate areas of dense sampling; large polygons reflect areas with more sparse sampling density. This method does not involve any smoothing and shows an undistorted picture of the value distribution across cortex.

Topographical surface reconstructions of response maps beyond CF are characterized by global gradients and by local scatter. Both properties can be evaluated quantitatively for each map. These estimates are computed based on a weighted least-squares linear regression model (Cleveland et al. 1993) of data points in the vicinity of each recording site. The size of the vicinity determines the steepness of the global gradients that can be identified. Based on the parameter distributions in cat (Schreiner and Sutter 1992; Sutter and Schreiner 1995) and owl monkey AI (Recanzone et al. 1999), the vicinity was selected to be 40% of the total data set (corresponding to $\text{span} = 0.4$) closest to the site. The weight for the least-squares fit is an exponential decay function for the relative contributions of neighboring data within the vicinity (Cleveland et al. 1993). This procedure quantifies the spatial orderliness of the estimated parameter (global gradients) and the unexplained residual variability (local scatter). This approach is selected because this technique is equivalent to the commonly applied local regression analysis of two-dimensional data sets and permits a direct quantitative assessment of the correspondence between the amount of variability explained by the local regression model and the degrees of freedom the model consumes (Hastie and Tibshirani 1995). A full account of the steps used to construct the response maps is given for one monkey (*sm1511*). Only raw data and response maps with their calculated spatial gradients are illustrated for the remaining three monkeys with intermediate steps omitted.

To quantify and compare the orientation of global parameter gradients, the axis of variation for CF and other response parameters is determined by computing gradient vectors for each recording site. Gradients are determined by evaluating the local slope in the regression model map. This is accomplished by computing vector components at each penetration site. Four points on the regression surface that surround the recording site delimit two orthogonal axes. The four points are positioned in a square configuration. The recording site is at its center and is separated radially from the surrounding four points by half the median distance of adjacent penetrations for that case. Vector summation of the two orthogonal components yields the direction of the local gradient. These local gradient vectors are accumulated for the whole map and plotted into a circular histogram or rose plot (Fisher 1993; Watson 1983), each bin covering 10° of arc. The standard rose plot of Watson (1983) and Fisher (1993) has been modified in this report where bin radius, rather than sector area, is proportional to the number of recording sites with the same gradient direction. Circular statistics are applied to quantify and compare global gradient direction(s) of several response parameters. This analysis discounts individual differences in the absolute parameter value and in the magnitude of the parameter gradient, which permit comparisons among animals. This is an important advantage because between animal differences are approximately of the same range of variation as within individual animals. More significantly, circular statistics permit a direct test against the null hypothesis that spatial organization of CF and other response parameters are not oriented and thereby, uniformly distributed.

TABLE 1. CF predicted by space across the plane of the cortex

Experiment	Factor	Dimensions	df	F	P	r ²	Magnification
sm1511	log ₂ (CF)	x, y	2	474	<0.001	0.89	0.84
sm1512	log ₂ (CF)	x, y	2	96	<0.001	0.59	0.67
sm881	log ₂ (CF)	x, y	2	102	<0.001	0.56	0.76
sm878	log ₂ (CF)	x, y	2	105	<0.001	0.70	0.61

P values from two-way ANOVA. F is the test statistic. df, degrees of freedom; r², spatial variability captured by linear regression model based on x and y dimensions; magnification, spatial assessment of cortical representation of CF values in octaves/mm.

tonotopic gradient reversal. The caudal boundary of AI is marked by a change in direction of tonotopy. For penetrations made in the supratemporal plane, higher CFs (above black dots in Fig. 1A) were encountered. These recording sites were more variable both in the plane of the cortex and in laminar depth and represent more ambiguous sites than those on the surface of the gyrus. The CF progression of sites on the supratemporal plane is consistent with AI and forms a continuous frequency representation when combined with sites on the temporal gyrus. Thus AI is not confined to the supratemporal plane. Rather, AI in the squirrel monkey has a component on the temporal

gyrus, which is similar to other New World monkeys (Aitkin et al. 1986; Imig et al. 1977; Luethke et al. 1989; Morel and Kaas 1992; Recanzone et al. 1999). The reconstructed response maps that follow are derived solely from recording sites on the lateral AI surface.

The cytoarchitectonic verification of AI, which is physiologically characterized by CFs higher rostrally (6 kHz) and lower caudally (3 kHz), spanning ~4 mm (as in all densely mapped cases) on the temporal gyrus in the rostrocaudal dimension, appears in Fig. 2. The illustrated case is a separate animal (Fig. 2; sm1510, male) dedicated to areal and laminar

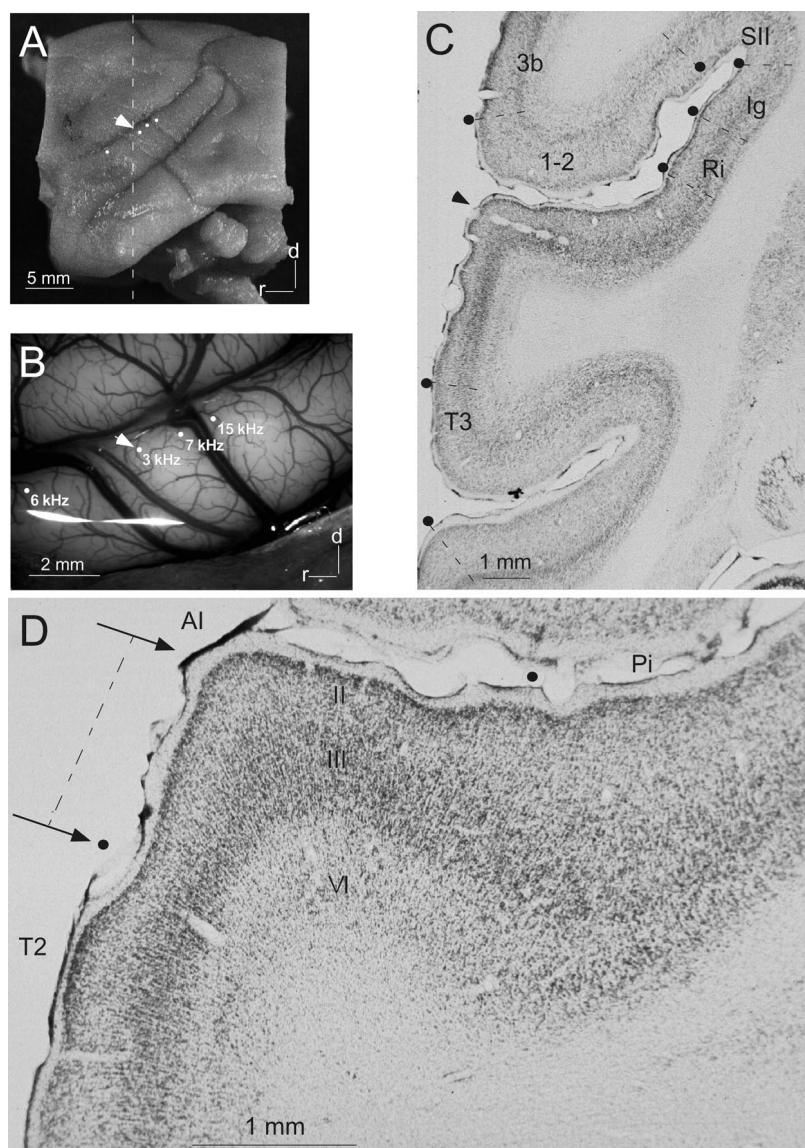


FIG. 2. Anatomical determination of AI. Nissl preparations show global view of recording sites and auditory cortical subdivisions in the squirrel monkey forebrain. A: the left hemisphere from which the recordings were made, after fixation. \circ , the site of 6-, 3-, 7-, and 15-kHz CF recordings, respectively, as shown in B. Δ (A–C), site of electrolytic lesions. - - -, the plane of section for D, which is slightly rostral to the lesions (Δ , C). The depressions running from rostradorsal to caudoventral between the \circ correspond to major cortical veins shown in the living specimen (B). The truncations at the caudal and rostral poles are blocking cuts that define the plane of section. Macrolens, 50 mm, 1:3.5. B: the recording sites projected onto a lateral view in the living specimen in a digitized image. Auditory cortex bounded by 3- and 6-kHz sites are within AI; 7 and 15 kHz may be within the posterior auditory field of Burton and Jones (1976). C: cytoarchitecture of adjoining nonauditory fields where boundaries are indicated by \bullet and - - -. The lesion (\blacktriangle) was made adjacent to CF = 3 kHz on the temporal gyrus, a physiological marker for the caudal sector of AI, and extended into the supratemporal plane to facilitate identification. Protocol for C: thionin stain, 50- μ m-thick section, planachromat, N. A. 0.08, \times 12. D: a transverse section showing AI and nearby fields. The characteristic features in AI are a well-developed layer I, a thin, intensely stained layer II, an unusually thick layer III, and a cell-sparse layer V. In the second temporal field (T2), layer II is not as thick, and the parainsular cortex (Pi) has a much more diffuse layer III. Subdivisions are derived from Burton and Jones (1976). The bracketed region, indicated by \rightarrow joined by - - -, is the portion of AI on the temporal gyrus targeted for mapping. Protocol as in C except for, planachromat, N. A. 0.04, \times 31.

analysis by minimizing the number of penetrations to identify AI physiologically. Dense mapping in other cases, while definitive for AI, nevertheless degraded the field's cytoarchitectural integrity substantially. In Fig. 2, auditory cortex caudal to the 3-kHz site appears to have a CF (7 and 15 kHz) gradient reversal, which may represent the posterior auditory field (Burton and Jones 1976; Jones and Burton 1976). Due to this possibility, all analyses were limited to data rostral to identifiable caudal CF gradient reversal to ensure that data interpretation was within AI. Figure 2, *A* and *B*, shows the recording sites superimposed on the fixed gross brain and in vivo photomicrograph, respectively. The arrowhead marks electrolytic lesions (Fig. 2, *A–C*) made adjacent to the 3-kHz penetration on the temporal gyrus. The lesion tract in Fig. 2*C* was extended into the supratemporal plane to facilitate its anatomic identification and does not imply that supratemporal AI was mapped. In Fig. 2*A*, --- marks the section plane for Fig. 2*D*, which is slightly rostral to the lesions. Based on laminar organization, subdivisions can be derived that are in close agreement with delineation of AI and surrounding fields in accordance to prior work (Burton and Jones 1976). Figure 2*C* illustrates the locations of these subdivisions. Boundaries are indicated by ● and ---. Figure 2*D* shows that AI has a well-developed layer I, a thin, densely stained layer II, an unusually thick layer III, and a cell-sparse layer V. It is apparent at this cross-sectional level (Fig. 2*D*) that ~40% of AI is located on the lateral surface of the temporal gyrus (bracketed region indicated by → joined by a ---) and ~60% is located on the supratemporal plane within the lateral sulcus. All physiological data presented in the next section were obtained from AI located on the temporal gyrus, which corresponds to the bracketed region of the temporal gyrus in Fig. 2*D*.

CF maps

Figure 1*B* is a CF tessellation map of neuronal clusters in AI on the temporal gyrus of *monkey sm1511*, with data from the AI portion replotted (Fig. 1*A*). Here CF is shown by a number plotted at the recording site and by a colored polygon surrounding each number. Tessellated spatial maps for CF and other response parameters are reconstructed by Voronoi-Dirichlet Tessellation (see METHODS). Each polygon represents the cortical area characterized by this recording site. The reconstructed polygon maps are plotted with the color coding for the value of the response parameter at the corresponding recording site. Comparison between the spatial distribution of the raw CF values (Fig. 1*A*) and the tessellated map (Fig. 1*B*) shows a direct correspondence of the two reconstructions. However, the tessellated map allows easy detection of parameter gradients and local discontinuities in the distribution of receptive field parameters.

From the tessellated map, the extent and range of frequency distribution in AI can be assessed. The isofrequency contours are 4 mm long, and the accessible frequency map is 2–3 mm in ventral to dorsal extent. The dorsal edge is bounded by the lateral sulcus (LS), corresponding to a CF of ~6 kHz. The ventral edge is limited by experimental choice (time constraint) to sample neurons with CFs >1 kHz; there are two locations with CFs of ~0.6 kHz, which is in close proximity to the ventral physiological border at 0.5 kHz (*sm1512* and *sm881*, Fig. 3) of the studied area. This map is highly structured with

orderly progression of CF values that follow a caudoventral to rostradorsal trajectory for successively higher CF values. The other three CF maps are structured similarly (Fig. 3) in the following manner. CF progression is smooth and continuous. AI is ~4 mm long in each experiment, with a dorsal to ventral extent of 2–3 mm; the actual extent of AI on the cortical surface may be greater since the ventral aspect was not explored fully. For *sm1511* and other animals, the systematic variation of CF across cortical surface is a dominant organization property. The CF maps differ among animals in the cortical magnification factor by $\leq 27\%$ (Table 1) and in the direction of the CF gradient by $\leq 53^\circ$ (see Table 5 and Fig. 13). Spatial position on the temporal gyrus accounts for 56–89% (Table 1) of CF variability when this strong feature is assessed with a model in which CF is dependent on a locally linear function of coordinate position. The null hypothesis is for CF to be randomly distributed; the model is statistically significant ($P < 0.001$).

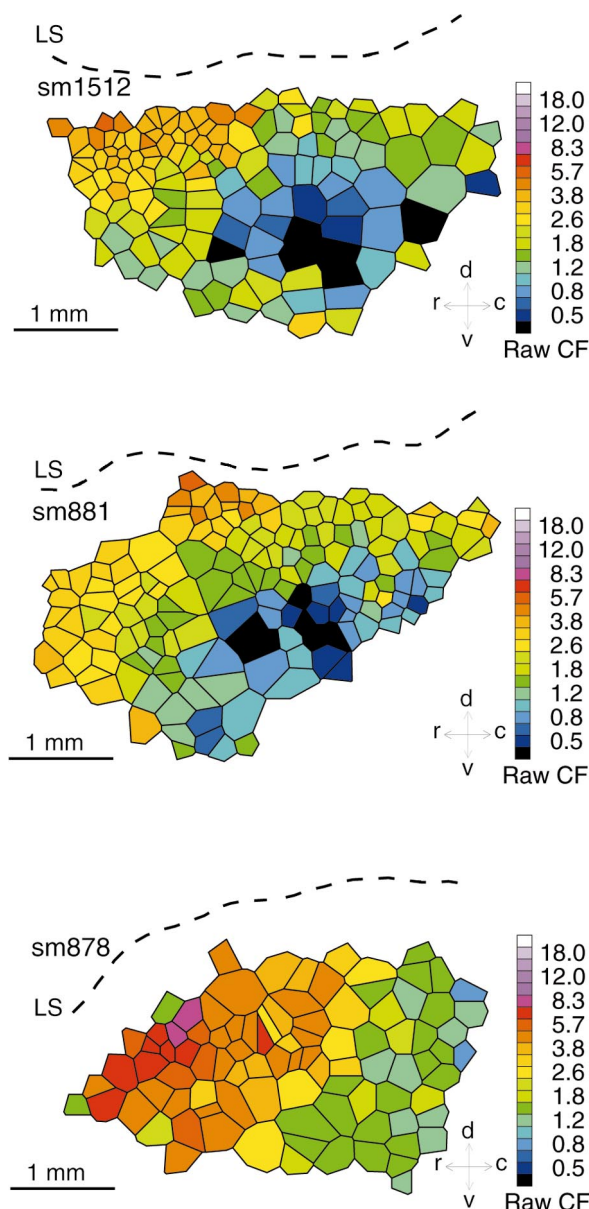


FIG. 3. CF maps for 3 other monkeys. LS, lateral sulcus.

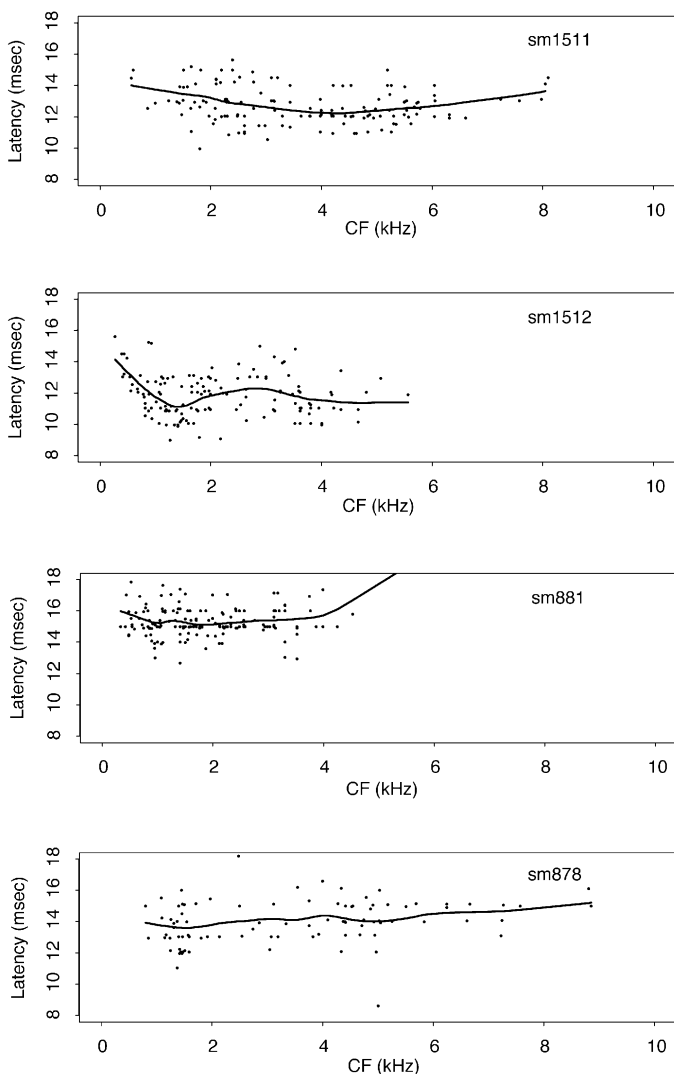


FIG. 4. Co-variation of latency and CF. —, the latency predicted by modeling this parameter as a locally linear function of CF.

Latency maps

Response latency is topographically organized in AI and varies monotonically along an axis nearly orthogonal to the tonotopic axis. CF correction is not applied to latency maps because the variability in latency is comparable to, or larger than, its correlation with CF. This is demonstrated in Fig. 4 by a nearly horizontal orientation of the local linear regression for all four cases. Only case *sm1512* shows a limited CF dependence of latency below ~ 1.5 kHz. Figure 5 illustrates tessellation maps for the latency parameter in *monkey sm1511*. A color-coded raw latency response map shows the spatial distribution of experimentally observed values (Fig. 5A). The nonparametric locally linear regression fit is shown in Fig. 5B. It reveals strong spatial coherence of latency values locally and a monotonic gradient of values along the rostrocaudal axis. Progressively longer latency values occupy rostral portions of the response map. Latency response maps for *monkeys sm1511* and *sm1512* are statistically significant ($P < 0.001$), and account for $\sim 50\%$ of the total variability (Table 2). While individual maps vary with respect to absolute latencies and orientation of the latency gradient, a global gradient is evident

in all maps (Figs. 5B and 6). In three monkeys, there is, in general, a global increase in latency values moving in the caudo-rostral axis. In *sm1512*, the gradient is rotated from low to high latency along the dorsoventral axis. The peak to trough latency (5th to 95th percentiles) gradient difference within individual animals is ~ 4 ms. One case (*sm881*) had overall longer latencies and a more restricted range.

Threshold maps

Minimum threshold, defined as the lowest SPL (fixed rise time of 3 ms) that evokes spike activity, is also organized topographically in AI. The raw thresholds are correlated with CF (Fig. 7); there is a global decrease of threshold with increasing CF. The spatial distribution of raw threshold at each recording site (Fig. 8A) is presented in the same format as that for CF (Fig. 1B). This map reflects the effect of co-variation between threshold and CF, with the highest thresholds at the caudoventral edge of the map that is also characterized by low CFs. Applying the decorrelation procedure to the raw threshold data removes this CF dependence. In Fig. 7, the fitted curves passing through data points are the expected thresholds for a given CF, as determined by a nonparametric, locally linear regression procedure. For threshold modeled by CF, the nonparametric locally linear regression fit is significant ($P < 0.01$ for all cases) and captures 37–68% of the total variability (Table 3). Residual, CF-independent threshold values are computed by subtracting the model from experimental data. The tessellated map of the residual threshold value at each recording site (*sm1511*, Fig. 8B) reveals a high degree of scatter; however, spatially segregated clusters of high and low threshold values can be discerned. This becomes more apparent after application of a locally linear regression model. It reveals that the residual threshold map is globally ordered with a largely monotonic gradient along the rostrocaudal axis (Fig. 8C). Higher residual threshold values are, on average, found at the caudal portion. While the regression fit is statistically significant, it captures only a relatively small proportion of the variance (see Table 4), indicating that the local scatter of residual threshold values is relatively high.

At the extreme rostral edge of the map (Fig. 8, B and C), some relatively high-threshold units demarcate a physiological border and hint at a gradient reversal. However, neurons immediately rostral to these border cells are either weakly driven or nonresponsive to tone and noise burst stimuli. If these cells are taken to mark the rostral AI physiologic border, then there is no residual threshold gradient reversal within AI. Figure 9 shows the CF-corrected threshold regression surfaces for three other monkeys. While individual maps vary in absolute threshold values, the global gradient is preserved, with residual threshold increasing along the rostral to caudal extent of AI. The orientation of threshold gradient in *case sm878* is less clear and appears to be rotated by $\sim 45^\circ$. The spatially limited rostral boundary effect of increased residual threshold is also seen in *monkeys sm1512* and *sm878*. The CF-corrected threshold surfaces are statistically significant ($P < 0.05$) and account for ~ 17 –33% of the total variability for threshold corrected for CF (Table 4). For residual threshold, the fluctuation range (5th to 95th percentiles) is 10 dB.

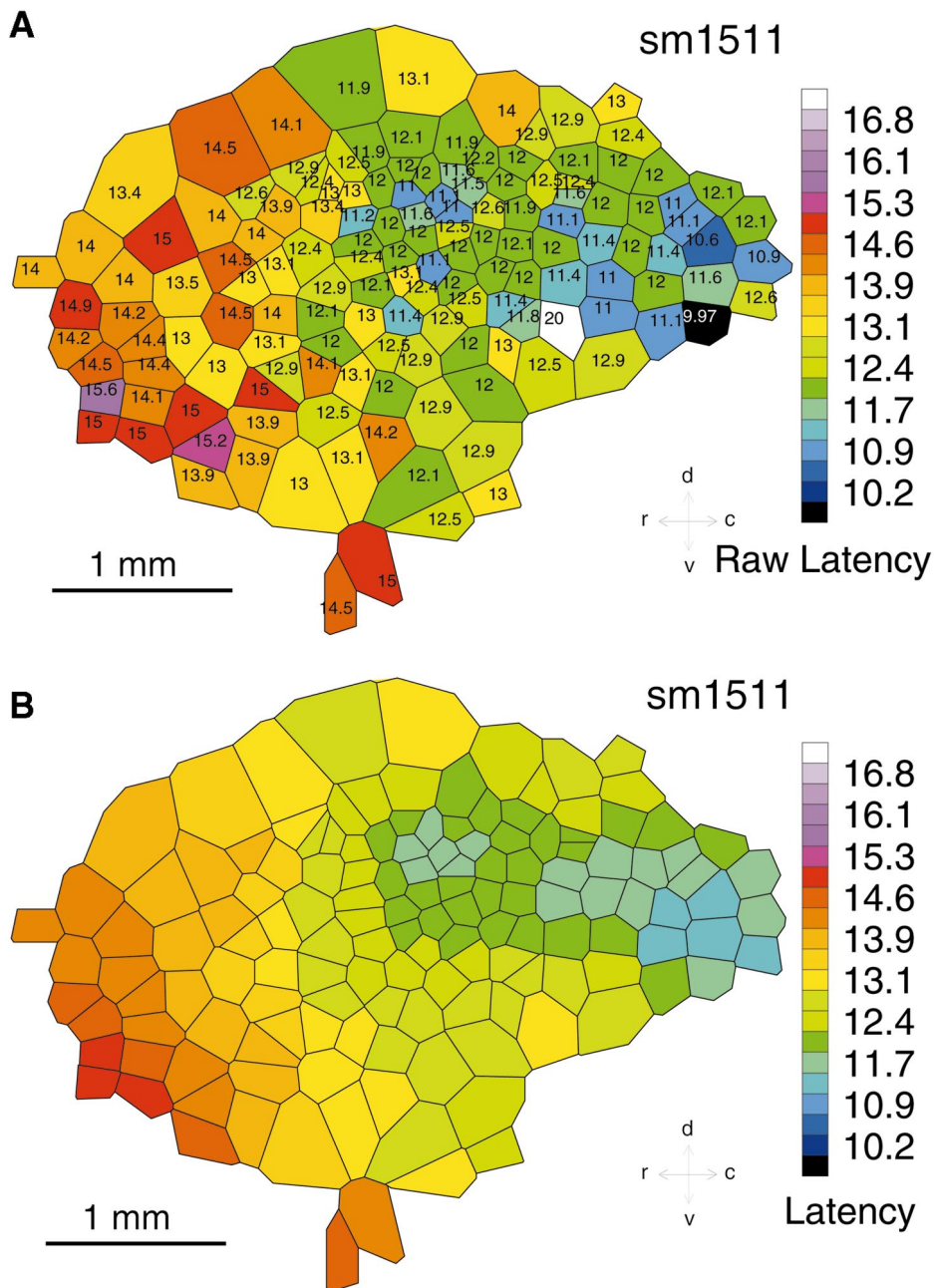


FIG. 5. Latency map for *sm1511*. *A*: raw latency. Observed minimum latency values for AI recording sites on the cortical surface are shown. The colored bar scale is in millisecond units. *B*: latency. The spatial variation of latency predicted by a locally linear regression model with predicted values represented by color only.

Q10 bandwidth maps

Sharpness of tuning shows clustering in AI, however, the maps are more variable than for the other response parameters and have direction changes in the gradient. There is a tendency for Q10 to be positively correlated with CF (Fig. 10), although this relationship does not always reach statistical significance (Table 3). Figure 11A is a tessellation map for raw Q10 values. The map shows two spatially segregated clusters of broadly tuned and two clusters of more narrowly tuned cortical locations. For *sm1511*, Q10 modeled by CF (Fig. 10, top) is significant ($P < 0.01$) and accounts for 34% of the total variability (Table 3). The CF decorrelation procedure does not

greatly affect the pattern of spatial variation (compare Fig. 11, A and B). Two regions of relatively narrow tuning (high Q10) interdigitate with areas of relatively broad tuning (low Q10). This spatial segregation is highlighted in the locally linear regression surface fitted to the residual Q10 data (Fig. 11C). In this animal, locally coherent residual Q10 values form contours across AI that are roughly orthogonal to the tonotopic axis. For *sm1511*, the regression map is statistically significant (Table 4, $P < 0.001$) and captures 25% of the residual Q10 variability. The spatial variation from peak to trough is ~ 3 Q units, comparable to the average in this experiment. Figure 12 shows residual Q10 maps for three other monkeys. In all three addi-

TABLE 2. Relationship between tone response latency and space across the plane of the cortex

Experiment	df	Effective df	F	P	Significance	Equiv r^2
sm1511	2	9.0	4.15	<0.001	***	0.54
sm1512	2	8.4	5.72	<0.001	***	0.46
sm881	2	7.9	3.08	0.003	**	0.15
sm878	2	8.7	1.36	0.221		0.18

P values from ANOVA. Effective df, neighborhood effects of locally linear regression fit increases the effective degrees of freedom; equiv r^2 , fraction of total variability captured by model, *** $P < 0.001$; ** $P < 0.01$.

tional cases, the topography for Q10 is patchy across AI and shows gradient reversals. The spatial variation for residual Q10 is more variable than the maps for CF, latency, and residual threshold. The fitted patterns of spatial variation reached statistical significance in three of four cases (Table 4, $P < 0.05$).

In all four animals, the distribution of Q values 30 dB above threshold also was analyzed. Since the spatial distribution results for Q30 were essentially identical to the findings for

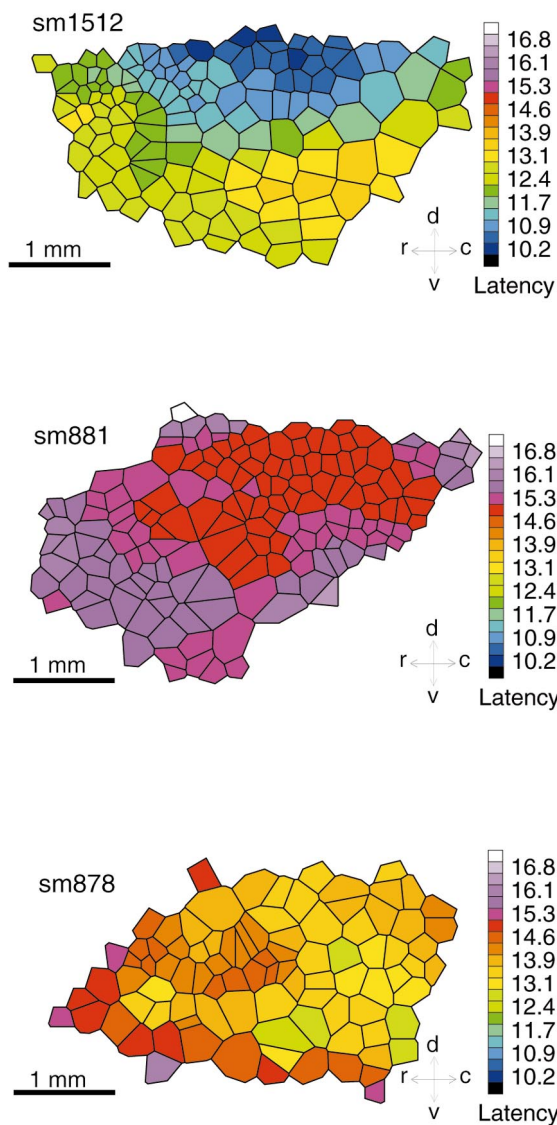


FIG. 6. Latency maps for 3 other monkeys.

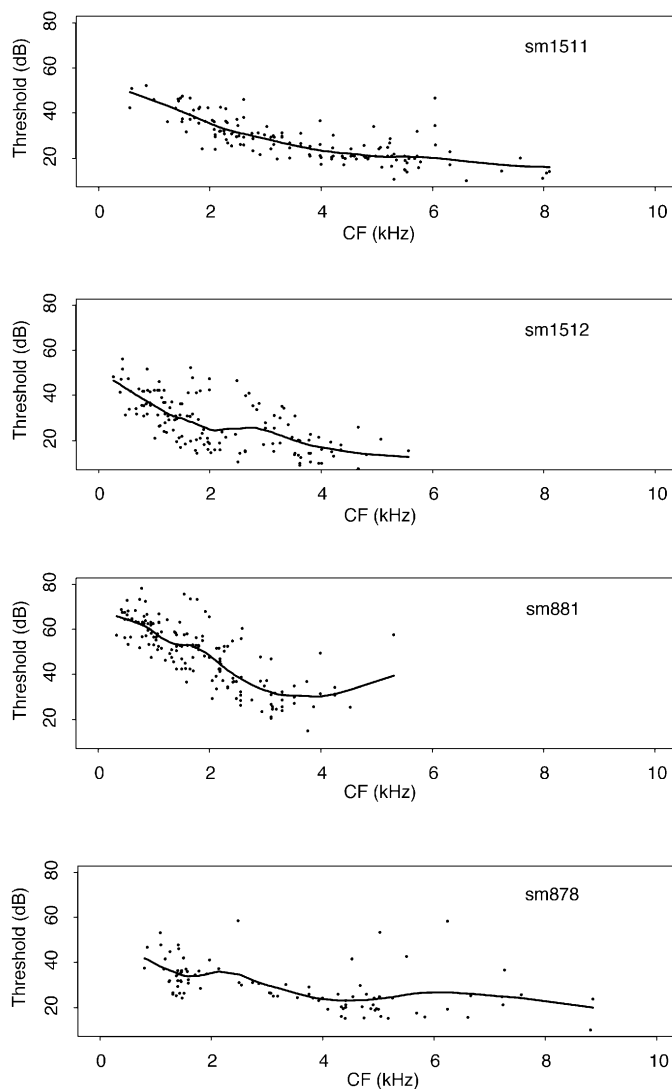


FIG. 7. Co-variation of threshold and characteristic frequency. —, the threshold predicted by modeling this parameter as a locally linear function of CF.

Q10, no details are shown. However, the results further support the conclusion drawn from Q10 that AI contains several spatial clusters of broadly and narrowly tuned neurons.

Spatial gradient of CF and other response parameters

The spatial distributions of response parameters show single (CF, latency, and threshold) or multiple (Q10) global gradients across AI. The patchy distribution of Q10 compared with the monotonic global gradients for the other three parameters suggests a systematic difference in the representational principles for the two parameter groups. Among the three parameters with monotonic gradients, the orientations of the gradients are not in the same direction. To quantify and compare the gradient orientations, the main axis of variation for CF and other response parameters is determined by accumulating gradient vectors for all recording sites in bins covering 10° of arc (Fig. 13). These modified rose plots (Fisher 1993; Watson 1983) are computed for CF, latency, residual threshold, and residual Q10 gradients. Dorsal and ventral directions are 0 and 180°, while rostral and caudal directions are 270 and 90°, respectively, on

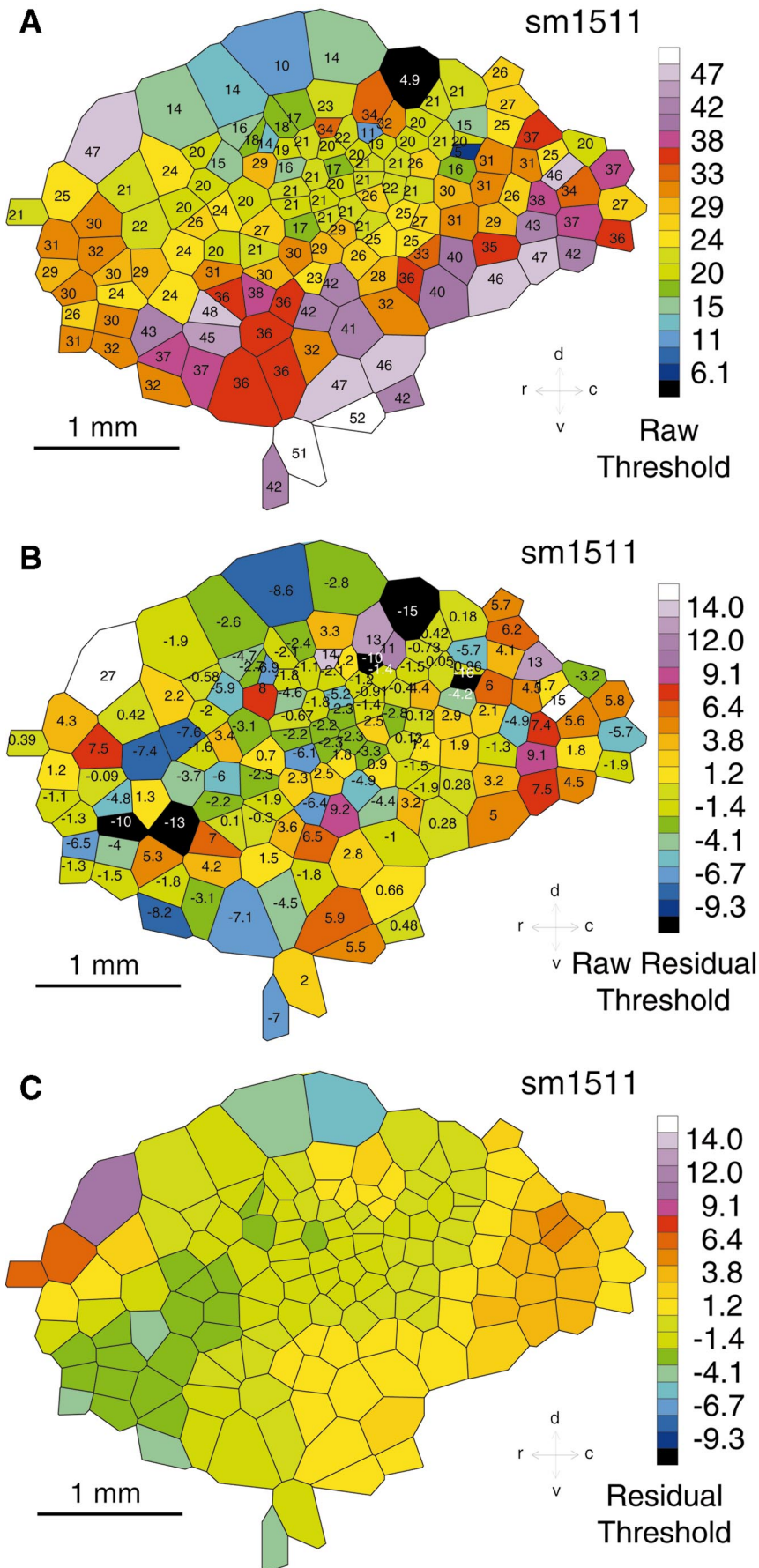


FIG. 8. Threshold map for *sm1511*. *A*: raw threshold. Observed threshold values for AI recording sites on the cortical surface are shown. The colored bar scale is in dB (SPL) units. *B*: raw residual threshold. Threshold to CF co-variation is accounted for by modeling the relationship with a locally linear regression procedure and subtracting the observed threshold by the predicted (CF dependent) value. The resultant raw residual threshold values are represented by a tessellated color map with CF-corrected threshold values embedded within polygons. *C*: residual threshold. The spatial variation of residual threshold predicted by a locally linear regression model, with predicted values represented by color only.

TABLE 3. Relationship between response parameters and CF

Experiment	df	Effective df	<i>F</i>	<i>P</i>	Significance	Equiv r^2
Threshold ~ CF						
<i>sm1511</i>	1	4.6	9.69	<0.001	***	0.66
<i>sm1512</i>	1	3.9	4.36	0.003	**	0.48
<i>sm881</i>	1	4.1	11.52	<0.001	***	0.68
<i>sm878</i>	1	4.4	3.78	0.005	**	0.37
Q10 ~ CF						
<i>sm1511</i>	1	4.6	4.30	0.002	**	0.34
<i>sm1512</i>	1	3.9	0.83	0.507		0.40
<i>sm881</i>	1	4.1	4.97	<0.001	***	0.28
<i>sm878</i>	1	4.2	1.91	0.113		0.35

P values from nonparametric ANOVA. CF, characteristic frequency. *** $P < 0.001$; ** $P < 0.01$.

the unit circle. The length of the arc radius is proportional to the number of observations. Contrary to the null hypothesis, gradients (Table 5) for all response parameters (residual Q10 for *sm878* is the only exception) are oriented.

In three of the four cases, the mean direction of the CF gradient is near 0° , i.e., oriented dorsally (see Fig. 13, ●, Table 5). In case *sm878*, the orientation is rotated by $\sim 40^\circ$, pointing more rostrally. Furthermore, the CF gradients reveal a single main component, expressed as a single lobe or wedge in the rose diagrams and by high vector strength values (Table 5), suggesting that all cases had a monotonic gradient. Case *sm1512* shows a small secondary lobe in the opposite direction of the main lobe. This small lobe likely reflects a reversal in tonotopic gradient near the ventral edge of the map (Fig. 3) and results in a reduced vector strength.

The modified rose diagrams for latency gradients show two main differences to CF gradients. First, the width of the lobes is broader and less direction specific, resulting in reduced vector strength values (Table 5), suggestive of a less strict overall gradient. Second, the mean direction of the latency gradient is significantly rotated (see Fig. 13, ●; $P < 0.05$) relative to the CF gradient by $\Delta \sim 88^\circ$ on average (Table 5). This confirms that CF and latency gradients are nearly orthogonal to each other, and the global components of the two response parameters are mapped independently. The axis of variation of the other response parameters also differs from the direction of the CF gradient.

The modified rose diagrams of residual threshold again show a fairly broad distribution of the local gradients, and potentially reveal several lobes (e.g., cases *sm1511* and *sm1512*). Nevertheless, a mean gradient direction can be defined for all cases that is different from that of the CF gradients ($\Delta \sim 90^\circ$) and the latency gradients ($\Delta \sim 166^\circ$) (Tables 5 and 6). The difference

between latency and residual threshold gradients is statistically significant to $P < 0.001$ in three of four monkeys (Table 6). Finally, the modified rose diagrams of Q10 gradients show two or three distinct lobes. This is due to the finding of several patches of narrowly and broadly tuned neurons (Figs. 11 and 12), resulting in multiple gradients and inherent gradient reversals. Accordingly, the resultant or mean vector length is fairly small and the difference to the CF gradient is statistically significant for one monkey only (Table 6). Similarly, the differences among Q10, latency, and threshold gradients are not well defined. However, the existence of multiple Q10 gradients alone demonstrates representational independence between Q10 and the other three parameters. Overall, this analysis shows the spatial and representational independence among the global parameter gradients in the four studied receptive field properties in squirrel monkey AI. However, it should be kept in mind that these global gradients capture less than half of the total variability of the parameters.

DISCUSSION

Information processing on an areal and laminar basis must contribute in fundamental ways to the structure of representational and computational maps that is a definitive feature of cortex (Knudsen et al. 1987; Kohonen and Hari 1999; Schreiner 1995). The robust expression of orderly CF representation in the cortex reflects the importance of frequency decomposition for analysis of the auditory scene evident at the sensory periphery. While CF is an important and conspicuous feature, this report presents evidence that other response parameters are also spatially organized in squirrel monkey AI. These are latency, CF-corrected threshold and CF-corrected

TABLE 4. Relationship of CF-corrected response parameters across the plane of the cortex

Experiment	df	Effective df	<i>F</i>	<i>P</i>	Significance	Equiv r^2
Threshold (corrected for CF) ~ <i>x</i> , <i>y</i>						
<i>sm1511</i>	2	9.0	2.46	0.012	*	0.17
<i>sm1512</i>	2	8.4	4.57	<0.001	***	0.27
<i>sm881</i>	2	7.9	2.09	0.041	*	0.32
<i>sm878</i>	2	8.9	3.71	<0.001	***	0.33
Q10 (corrected for CF) ~ <i>x</i> , <i>y</i>						
<i>sm1511</i>	2	9.0	4.92	<0.001	***	0.25
<i>sm1512</i>	2	8.4	3.27	0.002	**	0.21
<i>sm881</i>	2	7.9	4.44	<0.001	***	0.25
<i>sm878</i>	2	8.9	1.33	0.236		0.14

CF span = 0.4, space span = 0.4. *P* values from nonparametric ANOVA. *** $P < 0.001$; ** $P < 0.01$; * $P < 0.05$.

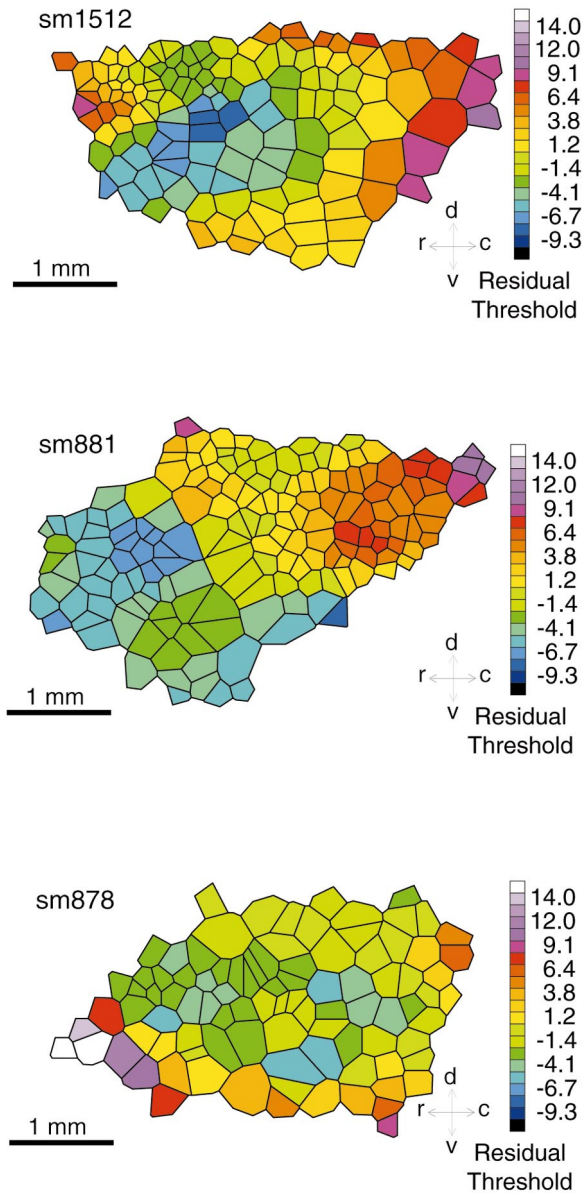


FIG. 9. Residual threshold maps for 3 other monkeys.

excitatory bandwidth. Understanding how the acoustic determinants of neuronal response change across the plane of the cortex relative to the CF axis is an essential step toward determining what acoustic features complement cortical frequency representation. These computational maps provide the substrate for efficient information processing, integration with other sensory modalities, and information extraction by higher order processing maps (Knudsen et al. 1987; Schreiner et al. 2000). Furthermore, the development of a more complete construct of AI functional organization has important implications for advancing our understanding how auditory cortex analyzes simple and complex sounds and how it reorganizes in auditory learning and in hearing loss.

AI location and borders

The location and extent of AI accessible on the lateral surface of the temporal lobe and orientation of the tonotopic

gradient varies within and across species (Aitkin et al. 1986; Imig et al. 1977; Luethke et al. 1985, 1989; Merzenich and Brugge 1973; Merzenich and Schreiner 1991; Merzenich et al. 1975; Morel and Kaas 1992; Morel et al. 1993; Recanzone et al. 1999). These spatial factors are important considerations for conducting particular classes of investigations in specific species. In the squirrel monkey, AI is relatively high on the temporal lobe. Much primary auditory cortex is accessible on the lateral surface of the temporal gyrus. This is in agreement with published accounts of squirrel monkey AI (Bieser and Mueller-Preuss 1996; Burton and Jones 1976; Funkenstein and Winter 1973; Jones and Burton 1976; Massopust et al. 1968; Winter and Funkenstein 1973) and other studies of New World monkey AI, such as the owl monkey (Imig et al. 1977; Morel and Kaas 1992; Recanzone et al. 1999), marmoset (Aitkin et al. 1986; Wang et al. 1995), and the tamarin (Luethke et al. 1989). The presence of AI straddling across both sides of the lateral fissure to include the temporal gyrus and supratemporal plane in the squirrel and other New World monkeys is in contradistinction to its complete supratemporal plane confinement in Old World monkeys (Merzenich and Brugge 1973; Morel et al. 1993; Rauschecker et al. 1997). Furthermore current results

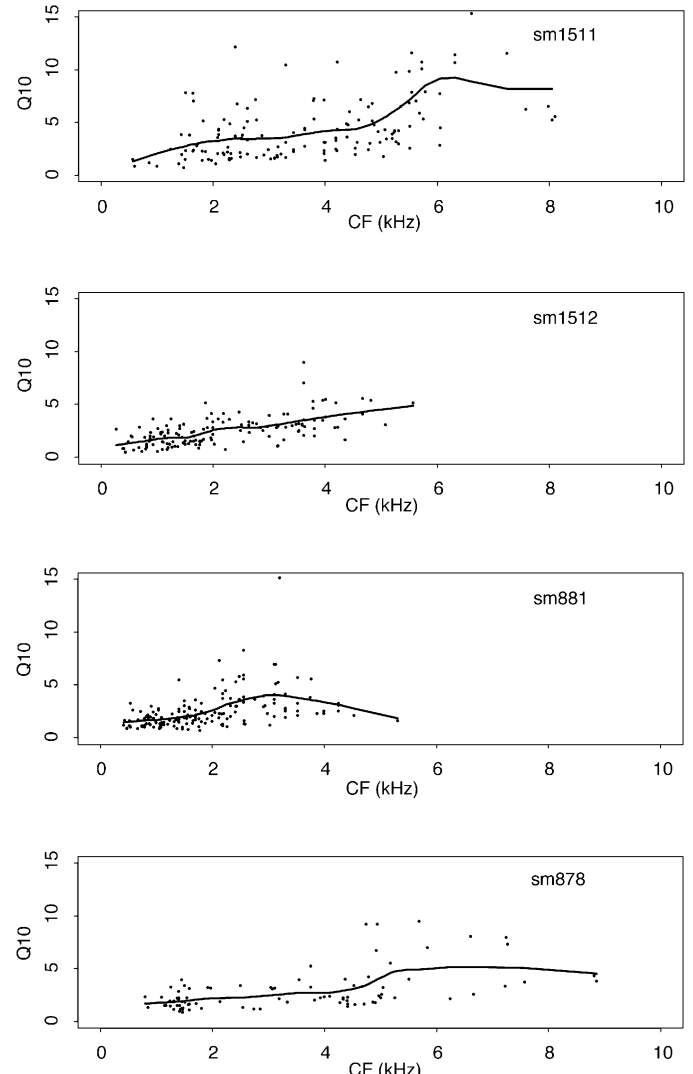


FIG. 10. Co-variation of Q10 and CF. —, the threshold predicted by modeling this parameter as a locally linear function of CF.

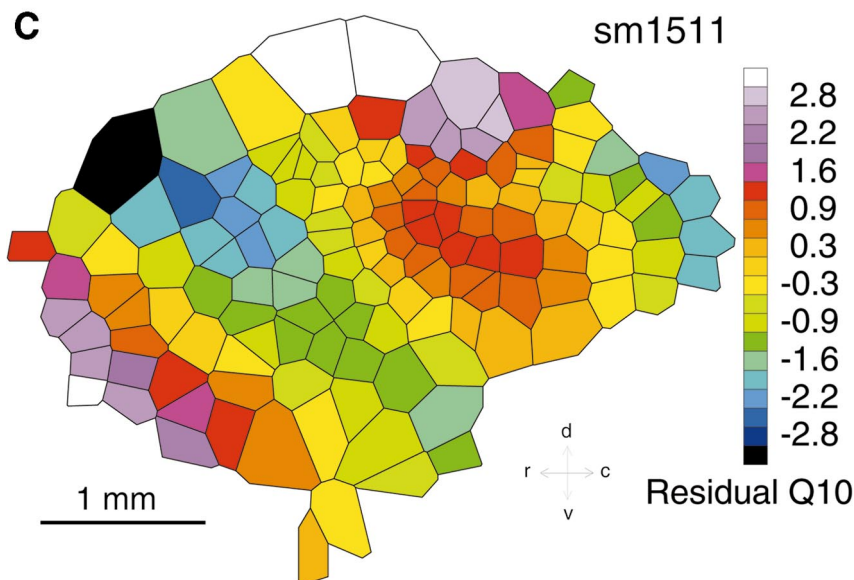
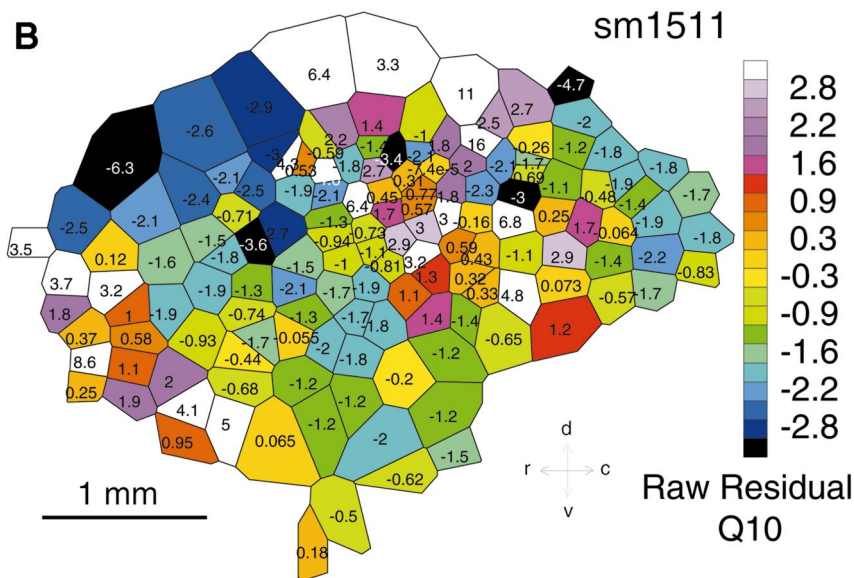
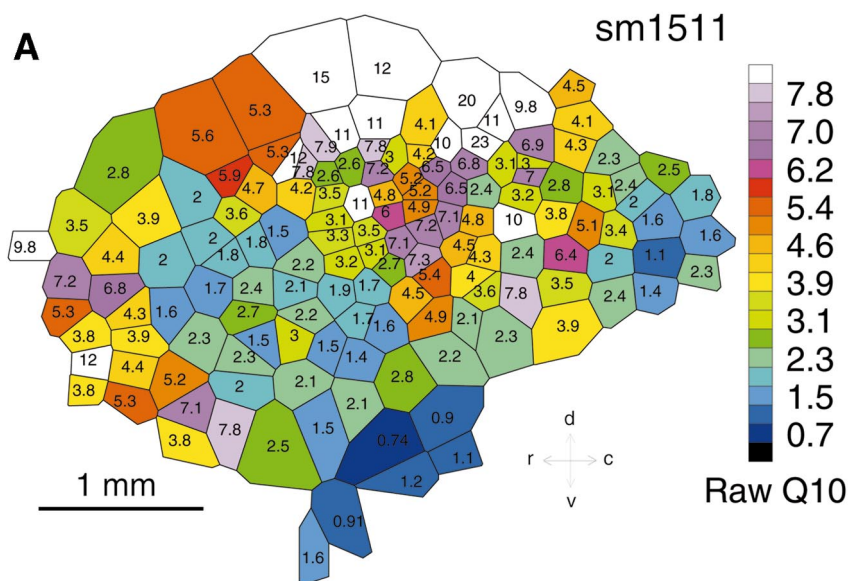


FIG. 11. Q10 map for *sm1511*. **A**: raw Q10. Observed Q10 values for AI recording sites on the cortical surface are shown. The colored bar scale is in dimensionless quality factor units. **B**: raw residual Q10. Q10 to CF co-variation is accounted for by modeling the relationship with a locally linear regression procedure and subtracting the observed Q10 by the predicted (CF dependent) value. The resultant raw residual Q10 values are represented by a tessellated color map with CF-corrected Q10 values embedded within polygons. **C**: residual Q10. The spatial variation of residual threshold predicted by a locally linear regression model, with predicted values represented by color only.

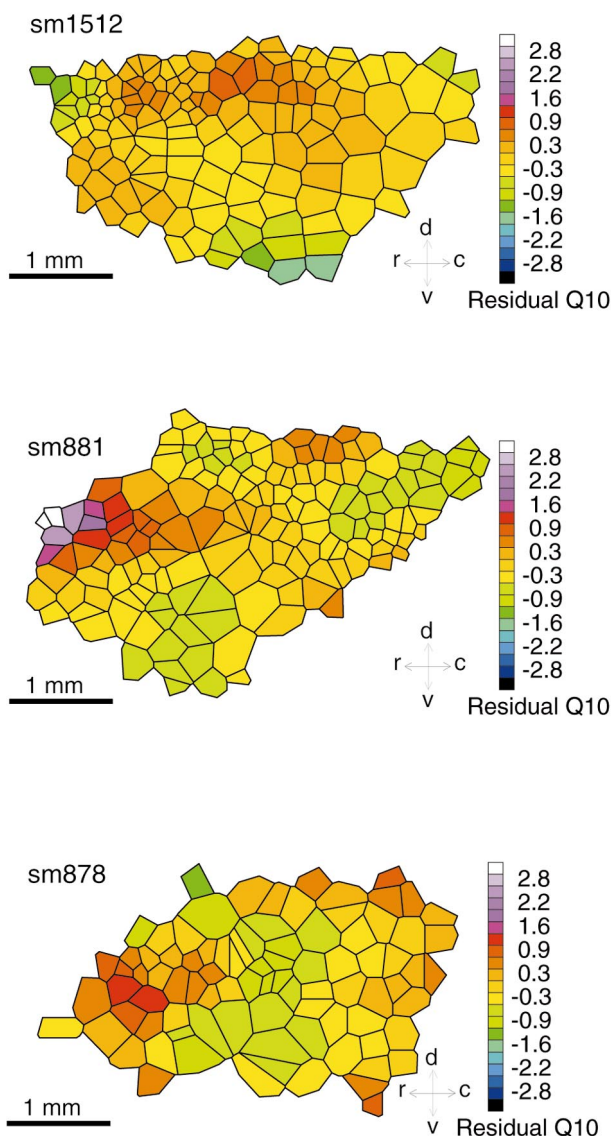


FIG. 12. Residual Q10 maps for 3 other monkeys.

confirm the cytoarchitectonic finding that AI extends from the supratemporal plane to the temporal gyrus (Burton and Jones 1976; Jones and Burton 1976) and the physiological result (Funkenstein and Winter 1973; Massopust et al. 1968; Winter and Funkenstein 1973) that AI on the temporal gyrus ranges from 0.5 to 6 kHz.

Two physiologic factors are used in this study to determine the rostrocaudal borders of AI: strength of response to pure tones and change in direction of tonotopic gradient. Near the rostral border, responses to pure tone stimuli are substantially weaker, despite a careful examination along the full extent of cortical columns. At some sites within the rostral border, the responses are too weak to determine a CF. The absent and/or relatively weak responses at the rostral aspect of AI are taken as a physiological border. Additionally, AI in virtually all mammalian auditory forebrains is the largest patch of cortex and CF distribution along this brain sector is highly regular (Winer 1992). For the squirrel monkey, the rate of CF change along the AI CF gradient vector is 0.6–0.8 octaves/mm (Table

1). Another criterion for demarcation is discontinuity of the AI monotonic CF gradient, which may manifest as spatially shifted, parallel duplication (Imig et al. 1977) or as directional reversal of the tonotopic axis in an adjacent field. The latter criteria were used to mark the macaque monkey (Kosaki et al. 1997; Merzenich and Brugge 1973; Morel et al. 1993; Rauschecker et al. 1997) AI/rostrolateral, the owl monkey (Imig et al. 1977) rostral/anterolateral, and squirrel (Luethke et al. 1988) AI/rostral borders, respectively, as well as in a number of other species, such as cat, rabbit, and guinea pig (Winer 1992). In squirrel monkey auditory cortex, the caudal AI physiological border is marked by apparent tonotopic gradient reversal. In this regard, the caudal field (Figs. 1A and 2B) is a candidate for the posterior auditory field (Burton and Jones 1976; Jones and Burton 1976). Another interpretation of the caudal field is that it is part of AI. In such an interpretation, higher CF isofrequency contours are assumed to be curvilinear, extend in and out of the supratemporal plane, and emerge along the rostral and caudal aspects of the lateral fissure on the temporal gyrus. Viewed from the lateral surface of the temporal lobe, this topographic scheme would give the impression of a CF gradient reversal in the rostrocaudal axis. This issue of designating the caudal field as a separate auditory sector or including it as a part of AI is not resolved in this paper and combined physiological and anatomical studies are needed to address this question. For the purpose of the present analysis of functional AI properties, the caudal aspect is excluded.

Gradients and coding

The three other response features in this study have topography distinct from the CF gradient. Latency and residual threshold have response maps that are nearly orthogonal to CF spatial organization. For residual bandwidth, the response maps have a few locally organized, coherent response values with multiple gradients and reversals. The spatial organization of these bandwidth clusters is individualized for each monkey. For threshold and bandwidth, the correction for CF co-variation of observed values to obtain residual values reveals response topographies beyond CF. Latency does not co-vary with CF appreciably in the studied frequency range, and its response map can be considered independent of CF. An important consideration is that there is no reason a priori to expect CF-corrected residual values to have any particular organized topography. The unequivocal demonstration of organized, functional topography for latency and threshold, and strong suggestion of spatial order for tuning bandwidth, is evidence that these three response parameters represent fundamental and independent dimensions for central representation of auditory stimuli (Schreiner 1995, 1998).

Latency is a dynamical factor that is related to how the response to an acoustic parameter, such as the envelope of tone burst stimuli, evolves in time (Heil and Irvine 1997). The gradient axis of organization for latency is different from the axis of organization for CF and residual threshold. Systematic variations in response latency may reflect several different aspects of sound coding. One role of latency variance may relate to coding of the temporal envelope slope in spectral profiles (Heil and Irvine 1997). Or it may be related to the coding of repetitive or sequential signals since latency can co-vary with the preferred repetition frequency of a neuron (Schreiner and

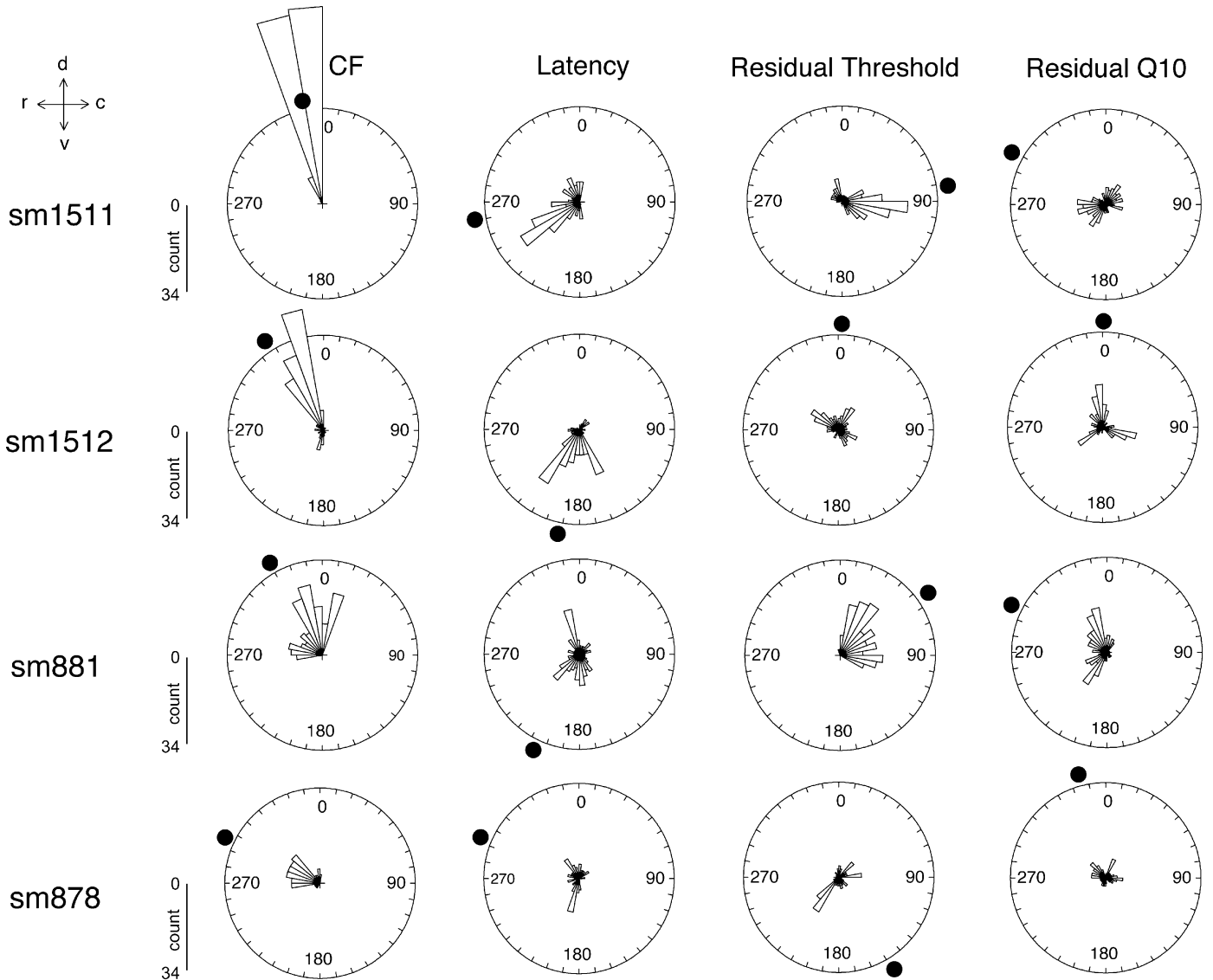


FIG. 13. Axes of variation for CF and other response parameters. Rose plots are computed for CF, latency, residual threshold, and residual Q10 gradients. Counts are the number of units that fall within an arc bin. ●, the mean angles.

TABLE 5. Response parameter gradient orientation significance, angles, and vector strengths

	Experiment	<i>n</i>	Significance	Mean Angle	Vector Strength
CF	<i>sm1511</i>	147	**	348.5	0.99
	<i>sm1512</i>	138	**	327.0	0.66
	<i>sm881</i>	163	**	330.4	0.83
	<i>sm878</i>	94	**	295.4	0.85
Latency	<i>sm1511</i>	147	**	259.6	0.62
	<i>sm1512</i>	138	**	192.0	0.65
	<i>sm881</i>	163	**	206.2	0.19
	<i>sm878</i>	94	**	292.9	0.24
Corrected threshold	<i>sm1511</i>	147	**	81.8	0.49
	<i>sm1512</i>	138	**	2.5	0.23
	<i>sm881</i>	163	**	54.4	0.83
	<i>sm878</i>	94	**	148.9	0.19
Corrected Q10	<i>sm1511</i>	147	**	296.6	0.19
	<i>sm1512</i>	138	**	0.7	0.18
	<i>sm881</i>	163	**	295.5	0.43
	<i>sm878</i>	88	**	344.5	0.11

** *P* < 0.01.

TABLE 6. Comparisons of response parameter gradients

	Latency	Corrected Threshold	Corrected Q10
CF			
<i>sm1511</i>	54.9***	209.7***	105.9***
<i>sm1512</i>	79.4***	11.6**	2.1 n.s.
<i>sm881</i>	19.0***	167.7***	4.1 n.s.
<i>sm878</i>	74.7***	79.2***	0.3 n.s. +
Latency			
<i>sm1511</i>		68.9***	3.8 n.s.
<i>sm1512</i>		52.3***	12.8**
<i>sm881</i>		39.5***	1.4 n.s.
<i>sm878</i>		7.8*	34.2 n.s. +
Corrected threshold			
<i>sm1511</i>			62.5***
<i>sm1512</i>			0.1 n.s.
<i>sm881</i>			32.7***
<i>sm878</i>			34.5 n.s. +

Yr (not shown) is the test statistic for each comparison. *** $P < 0.001$; ** $P < 0.01$; * $P < 0.05$; n.s., not significant ($P > 0.05$); +, corrected Q10 for *sm878* is not oriented, see Table 5.

Raggio 1996). Either scenario suggests that AI contains a systematic spatial representation of temporal signal features in addition to spectral features, such as CF and bandwidth. A companion study on AI responses to click train stimuli characterizes temporal response properties in more detail.

Variations in response threshold and response nonmonotonicity have been proposed to be substrates for intensity coding (Heil et al. 1994; Merzenich and Brugge 1973; Schreiner et al. 1992). As sound intensity increases, new cortical neurons are recruited, while others stop responding. Since the CF-corrected threshold, or residual threshold, varies monotonically along an axis roughly orthogonal to the CF axis, AI may be performing frequency and amplitude decompositions along these isofrequency contours. However, recent re-evaluations of the interactions between changes in sound intensity and temporal properties of stimulus onset (Heil 1997; Heil and Irvine 1997) suggest that systematic variations in response sensitivity may be more a reflection of the coding of dynamic stimulus aspects than overall intensity.

The observed cyclic variation of tuning bandwidth adds another coding dimension that is independent from CF, latency, and threshold. Cyclic or repetitive variation of response parameters such as Q10 overlaying other, monotonic parameter gradients gives rise to many different parameter combinations of the varying factors and is a hallmark of organization in visual cortex. Multiple overlying maps of independent coding dimensions follow naturally from principles of self-organizing processes and are characterized by a variety in gradient slopes, angles, and reversals (Kohonen and Hari 1999; Schreiner 1995, 1998). The finding of a systematically varying receptive field bandwidth supports the notion of a modular organization of frequency integration at the level of auditory cortex (Schreiner et al. 2000), with important implications for the analysis of acoustic scenes.

An interesting observation in this study is clear inter-individual variations in the organization of different animals. Similar variations have been observed in previous studies of primates (Recanzone et al. 1993, 1999) and cats (Heil et al. 1992, 1994; Mendelson et al. 1997; Raggio and Schreiner 1999). Despite these variations, global features of the maps and their interrelationships, such as the slope and relative angle of the

different gradients remain rather constant across animals. Furthermore, a recent mapping study of AI in owl monkeys (Recanzone et al. 1999) indicated that hemispheric differences in the cortical maps of a given animal are much smaller than differences between animals. This suggests that the observed inter-individual variability may be a reflection of the auditory history and experience of each animal (Merzenich et al. 1987) rather than random variations in the development of these maps or deficits in the applied mapping methodologies. Complicating this issue is the relative large local scatter that remains after removing the global gradients from the data. The large local scatter suggests influence by other organizational principles beyond low-dimensional topographies. Among the contributing factors to the scatter are likely systematic effects such as local cell composition and intracortical connections as well as variability of responses parameters in cortical depth and position.

The organizational patterns observed in the squirrel monkey share a number of similarities to patterns found in cat (Heil et al. 1992, 1994; Mendelson et al. 1997; Schreiner and Mendelson 1990; Sutter and Schreiner 1995) and owl monkey AI (Recanzone et al. 1999). In these species, there was supportive evidence for latency, threshold, and sharpness of tuning to be independently organized from CF and from each other as expressed by differences in their steepness and direction of local parameter gradients. However, details of the relationships among different parameters vary in the three species. For example, the latency gradient in cat AI (Mendelson et al. 1997) was found to be quite variable, weak, and nonmonotonic relative to the one seen in the squirrel monkey. The latency gradient in the owl monkey (Recanzone et al. 1999) was also less clearly evident compared with this study but appeared monotonic in some animals. Sharpness of tuning gradients was more clearly expressed in cat (Schreiner and Mendelson 1990) and owl monkey (Recanzone et al. 1999) than in the squirrel monkey. Overall, the global similarity among cat, owl monkey, and squirrel monkey cortical organization strengthens the hypothesis that the observed spatial variations and overlays of response parameters are a general principle of auditory cortical organization, including humans. The details of interspecies differences in functional organization may reflect differences in species-specific sound environments and in the behavioral role of different sound features.

Multiunit mapping

The experimental approach embraced in this study is acquisition of data from as many sites within a single animal as possible to permit analysis of patterns of spatial variations of response parameters. A consequence of this focus is that single and multiunits are accepted in our data set without prejudice. Eggermont's (1996) study examined the CF, minimum latency, minimum response threshold, and bandwidth of collections of single-unit spike trains recorded simultaneously from a single electrode and showed that these response parameters are highly correlated, suggesting responses to tone burst stimuli are globally homogeneous. While this conclusion cannot be inferred for individual sites (Schreiner and Mendelson 1990; Schreiner and Sutter 1992), the inclusion of multiunit recordings is unlikely to alter conclusions regarding global functional organization.

Anesthesia

These experiments were conducted under pentobarbital anesthesia. Auditory evoked responses under this regimen differ from those in awake animals, particularly with respect to temporal profile of responses to sustained stimuli but also with regard to latency (Schulze and Langner 1997). In this study, the responses are phasic and devoid of ongoing activity to steady tones. By contrast, awake monkeys show an increased number of tonic responses to ongoing sounds (Bieser and Mueller-Preuss 1996; deCharms et al. 1998). Despite this difference, the present conclusions are largely unaffected because basic organizational features in primary sensory cortex are not masked by pentobarbital anesthesia (Stryker et al. 1987). In visual cortex, the responses of neurons that code for sharpness of spatial contrast is modulated by the anesthetic state; however, basic response features such as ocular dominance, retinotopy, and orientation tuning are largely unaffected by anesthetic state. Likewise, the global spatial structure of latency, threshold, and bandwidth variations are unlikely to be substantially affected by anesthesia while some relative value differences to awake recordings may be present.

Conclusions

AI and adjacent temporal fields analyze and represent the auditory scene by decomposing it into independent stimulus components, including frequency, bandwidth, intensity/envelope dynamics, timing, and binaural properties. The exact nature, and especially the interactions, of these representational components is not completely understood. However, a consistent picture of a distributed sound representation along several independent base dimensions is emerging from studies in different species (Schreiner 1998). The squirrel monkey is a promising model to address these and other issues because it offers edge to edge isofrequency bands on the surface of the gyrus to support large scale parallel recordings, and it has the critical low-frequency neurons important in human speech representation. Furthermore the squirrel monkey has a rich history of awake cortical recordings in studies of species-specific vocalizations and is amenable to behavioral training. This New World monkey is an attractive model for future work in the primate auditory forebrain.

We thank D. Larue and J. Winer for generous help with anatomic analysis and construction of Fig. 2, B. Bonham for assistance with recording experiments, and S. Davies for the software for the rose diagrams.

This research was supported by National Institutes of Health Grants F32NS-09708 and VA Medical Research (S. W. Cheung), DC-02260, NS-34835 (C. E. Schreiner), and NS-10414; The Montgomery Street Foundation; The Coleman Fund; and Hearing Research, Incorporated.

REFERENCES

- AITKIN LM, MERZENICH MM, IRVINE DRF, CLAREY JC, AND NELSON JE. Frequency representation in auditory cortex of the common marmoset (*Callithrix jacchus jacchus*). *J Comp Neurol* 252: 175–185, 1986.
- BIESER A. Processing of twitter-call fundamental frequencies in insula and auditory cortex of squirrel monkeys. *Exp Brain Res* 122: 139–148, 1998.
- BIESER A AND MUELLER-PREUSS P. Auditory responsive cortex in the squirrel monkey—neural responses to amplitude-modulated sounds. *Exp Brain Res* 108: 273–284, 1996.
- BURTON H AND JONES EG. The posterior thalamic region and its cortical projection in new world and old world monkeys. *J Comp Neurol* 168: 249–302, 1976.
- CLAREY JC, BARONE P, AND IMIG TJ. Physiology of thalamus and cortex. In: *The Mammalian Auditory Pathway: Neurophysiology*, edited by Popper AN and Fay RR. New York: Springer-Verlag, 1992, p. 232–334.
- CLAREY JC, BARONE P, AND IMIG TJ. Functional organization of sound direction and sound pressure level in AI of the cat. *J Neurophysiol* 72: 2383–2405, 1994.
- CLEVELAND WS, GROSSE E, AND SHYU W. Local regression models. In: *Statistical Models in S*, edited by Chambers JM and Hastie TJ. New York: Chapman and Hall, 1993, p. 309–376.
- DECHARMS RC, BLAKE DT, AND MERZENICH MM. Optimizing sound features for cortical neurons. *Science* 280: 1439–1443, 1998.
- EGGERMONT JJ. How homogeneous is cat primary cortex? Evidence from simultaneous single-unit recordings. *Auditory Neurosci* 2: 79–96, 1996.
- FISHER NI. *Statistical Analysis of Circular Data*. New York: Cambridge, 1993.
- FUNKENSTEIN HH AND WINTER P. Responses to acoustic stimuli of units in the auditory cortex of awake squirrel monkeys. *Exp Brain Res* 18: 464–488, 1973.
- HASTIE T AND TIBSHIRANI R. Generalized additive models for medical research [see comments]. *Stat Methods Med Res* 4: 187–196, 1995.
- HEIL P. Auditory onset responses revisited. I. First-spike timing. *J Neurophysiol* 77: 2616–2641, 1997.
- HEIL P AND IRVINE DRF. First-spike timing of auditory-nerve fibers and comparison with auditory cortex. *J Neurophysiol* 78: 2438–2454, 1997.
- HEIL P, RAJAN R, AND IRVINE DRF. Sensitivity of neurons in cat primary auditory cortex to tones and frequency-modulated stimuli. II. Organization of response properties along the “isofrequency” dimension. *Hear Res* 63: 135–156, 1992.
- HEIL P, RAJAN R, AND IRVINE DRF. Topographic representation of tone intensity along the isofrequency axis of cat primary auditory cortex. *Hear Res* 76: 188–202, 1994.
- HIND JE CITED IN WOOLSEY CN. Tonotopic organization of the auditory cortex. In: *Physiology of the Auditory System, A Workshop*, edited by Sachs MB. Baltimore: National Education Consultants, 1972, p. 271–282.
- IMIG TJ AND ADRIÁN HO. Binaural columns in the primary field (A1) of cat auditory cortex. *Brain Res* 138: 241–257, 1977.
- IMIG TJ, RUGGERO MA, KITZES LM, JAVEL E, AND BRUGGE JF. Organization of auditory cortex in the owl monkey (*Aotus trivirgatus*). *J Comp Neurol* 171: 111–128, 1977.
- JONES EG AND BURTON H. Areal differences in the laminar distribution of thalamic afferents in cortical fields of the insular, parietal, and temporal regions in primates. *J Comp Neurol* 168: 197–248, 1976.
- KELLY JB AND JUDGE PW. Binaural organization of primary auditory cortex in the ferret (*Mustela putorius*). *J Neurophysiol* 71: 904–913, 1994.
- KNIGHT PL. Representation of the cochlea within the anterior auditory field (AAF) of the cat. *Brain Res* 130: 447–467, 1977.
- KNUDSEN EI, DU LAC S, AND ESTERLY SD. Computational maps in the brain. *Annu Rev Neurosci* 10: 41–65, 1987.
- KOHONEN T AND HARI R. Where the abstract feature maps of the brain might come from. *Trends Neurosci* 22: 135–139, 1999.
- KOSAKI H, HASHIKAWA T, HE J, AND JONES EG. Tonotopic organization of auditory cortical field delineated by parvalbumin immunoreactivity in macaque monkeys. *J Comp Neurol* 386: 304–316, 1997.
- LUETHKE LE, KRUBITZER LA, AND KAAS JH. Cortical connections of electrophysiologically and architectonically defined subdivisions of auditory cortex in squirrels. *J Comp Neurol* 268: 181–203, 1988.
- LUETHKE LE, KRUBITZER LA, AND KAAS JH. Connections of primary auditory cortex in the new world monkey (*Saguinus*). *J Comp Neurol* 285: 487–513, 1989.
- MASSOUST LC, WOLIN LR, AND KADOYA S. Evoked responses in the auditory cortex of the squirrel monkey. *Exp Neurol* 21: 35–40, 1968.
- MENDELSON JR, SCHREINER CE, AND SUTTER ML. Functional topography of cat primary auditory cortex: response latencies. *J Comp Physiol [A]* 181: 615–633, 1997.
- MERZENICH MM AND BRUGGE JF. Representation of the cochlear partition of the superior temporal plane of the macaque monkey. *Brain Res* 50: 275–296, 1973.
- MERZENICH MM, KAAS JH, AND ROTH GL. Auditory cortex in the grey squirrel: tonotopic organization and architectonic fields. *J Comp Neurol* 166: 387–401, 1976.
- MERZENICH MM, KNIGHT PL, AND ROTH GL. Representation of cochlea within primary auditory cortex in the cat. *J Neurophysiol* 38: 231–249, 1975.
- MERZENICH MM AND SCHREINER CE. Mammalian auditory cortex—some comparative observations. In: *The Evolutionary Biology of Hearing*, edited

- by Webster DB, Fay RR, and Popper AN. Berlin: Springer-Verlag, 1992, p. 673–689.
- MIDDLEBROOKS JC, DYKES RW, AND MERZENICH MM. Binaural response-specific bands in primary auditory cortex (AI) of the cat: topographical organization orthogonal to isofrequency contours. *Brain Res* 181: 31–48, 1980.
- MOREL A, GARRAGHTY PE, AND KAAS JH. Tonotopic organization, architectonic fields, and connections of auditory cortex in macaque monkeys. *J Comp Neurol* 335: 437–459, 1993.
- MOREL A AND KAAS JH. Subdivisions and connections of auditory cortex in owl monkeys. *J Comp Neurol* 318: 27–63, 1992.
- NEWMAN JD AND SYMMES D. Arousal effects on unit responsiveness to vocalizations in squirrel monkey auditory cortex. *Brain Res* 78: 125–138, 1974.
- NEWMAN JD AND SYMMES D. Feature detection by single units in squirrel monkey auditory cortex. *Exp Brain Res Suppl* 2: 140–145, 1979.
- PELLEG-TOIBA R AND WOLLBERG Z. Tuning properties of auditory cortex cells in the awake squirrel monkey. *Exp Brain Res* 74: 353–364, 1989.
- PHILLIPS DP AND IRVINE DR. Properties of single neurons in the anterior auditory field (AAF) of cat cerebral cortex. *Brain Res* 248: 237–244, 1982.
- PHILLIPS DP AND IRVINE DR. Some features of binaural input to single neurons in physiologically defined area AI of cat cerebral cortex. *J Neurophysiol* 49: 383–395, 1983.
- PHILLIPS DP AND ORMAN SS. Responses of single neurons in posterior field of cat auditory cortex to tonal stimulation. *J Neurophysiol* 51: 147–163, 1984.
- RAGGIO MW AND SCHREINER CE. Neuronal responses in cat primary auditory cortex to electrical cochlear stimulation. III. Activation patterns in short- and long-term deafness. *J Neurophysiol* 82: 3506–3526, 1999.
- RAUSCHECKER JP, TIAN B, AND HAUSER M. Processing of complex sounds in the macaque nonprimary auditory cortex. *Science* 268: 111–114, 1995.
- RAUSCHECKER JP, TIAN B, PONS T, AND MISHKIN M. Serial and parallel processing in rhesus monkey auditory cortex. *J Comp Neurol* 382: 89–103, 1997.
- REALE RA AND IMIG TJ. Tonotopic organization in auditory cortex of the cat. *J Comp Neurol* 192: 265–291, 1980.
- RECANZONE GH, SCHREINER CE, AND MERZENICH MM. Plasticity in the frequency representation of primary auditory cortex following discrimination training in adult owl monkeys. *J Neurosci* 13: 87–103, 1993.
- RECANZONE GH, SCHREINER CE, SUTTER ML, BEITEL RE, AND MERZENICH MM. Functional organization of spectral receptive fields in the primary auditory cortex of the owl monkey. *J Comp Neurol* 415: 460–481, 1999.
- ROUILLER EM, SIMM GM, VILLA AEP, DE RIBPAUPIERRE Y, AND DE RIBPAUPIERRE F. Auditory corticocortical interconnections in the cat: evidence for parallel and hierarchical arrangement of the auditory cortical area. *Exp Brain Res* 86: 483–505, 1991.
- SCHREINER CE. Functional topographies in the primary auditory cortex of the cat. *Acta Otolaryngol Suppl* 491: 7–15, 1991.
- SCHREINER CE. Order and disorder in auditory cortical maps. *Curr Opin Neurobiol* 5: 489–496, 1995.
- SCHREINER CE. Spatial distribution of responses to simple and complex sounds in the primary auditory cortex. *Audiol Neurootol* 3: 104–122, 1998.
- SCHREINER CE AND CYNADER MS. Basic functional organization of second auditory cortical field (AII) of the cat. *J Neurophysiol* 51: 1284–1305, 1984.
- SCHREINER CE AND MENDELSON JR. Functional topography of cat primary auditory cortex: distribution of integrated excitation. *J Neurophysiol* 64: 1442–1459, 1990.
- SCHREINER CE, MENDELSON JR, AND SUTTER ML. Functional topography of cat primary auditory cortex: representation of tone intensity. *Exp Brain Res* 92: 105–122, 1992.
- SCHREINER CE AND RAGGIO MW. Neuronal responses in cat primary auditory cortex to electrical cochlear stimulation. II. Repetition rate coding. *J Neurophysiol* 75: 1283–1300, 1996.
- SCHREINER CE, READ HL, AND SUTTER ML. Modular organization of frequency integration in primary auditory cortex. *Annu Rev Neurosci* 23: 501–529, 2000.
- SCHREINER CE AND SUTTER ML. Topography of excitatory bandwidth in cat primary auditory cortex: single-neuron versus multiple-neuron recordings. *J Neurophysiol* 68: 1487–1502, 1992.
- SCHULZE H AND LANGNER G. Periodicity coding in the primary auditory cortex of the mongolian gerbil (*Meriones unguiculatus*): two different coding strategies for pitch and rhythm? *J Comp Physiol [A]* 181: 651–663, 1997.
- SHAMMA SA AND SYMMES D. Patterns of inhibition in auditory cortical cells in awake squirrel monkeys. *Hear Res* 19: 1–13, 1985.
- STRYKER MP, JENKINS WM, AND MERZENICH MM. Anesthetic state does not affect the map of the hand representation within area 3b somatosensory cortex in owl monkey. *J Comp Neurol* 258: 297–303, 1987.
- SUTTER ML AND SCHREINER CE. Physiology and topography of neurons with multi-peaked tuning curves in cat primary auditory cortex. *J Neurophysiol* 65: 1207–1226, 1991.
- SUTTER ML AND SCHREINER CE. Topography of intensity tuning in cat primary auditory cortex: single-neuron versus multiple-neuron recordings. *J Neurophysiol* 73: 190–204, 1995.
- WANG X, MERZENICH MM, BEITEL R, AND SCHREINER CE. Representation of a species-specific vocalization in the primary auditory cortex of the common marmoset: temporal and spectral characteristics. *J Neurophysiol* 74: 2685–2706, 1995.
- WATSON GS. *Statistics on Spheres*. New York: Wiley, 1983.
- WINER JA. The functional architecture of the medial geniculate body and the primary auditory cortex. In: *The Mammalian Auditory Pathway: Neuroanatomy*, edited by Webster DB, Popper AN, and Fay RR. New York: Springer-Verlag, 1992, p. 222–409.
- WINTER P AND FUNKENSTEIN HH. Response properties of auditory cortical cells. *Brain Res* 31: 368, 1971.
- WINTER P AND FUNKENSTEIN HH. The effect of species-specific vocalization on the discharge of auditory cortical cells in the awake squirrel monkey (*Saimiri sciureus*). *Exp Brain Res* 18: 489–504, 1973.
- WOOLSEY CN AND WALZL EM. Topical projection of nerve fibers from local regions of the cochlea to the cerebral cortex of the cat. *Bull Johns Hopkins Hosp* 71: 315–344, 1942.